Friction Welding of Al-Al, Al-Steel, and Steel-Steel Samples

A.Z. Sahin, B.S. Yilbas, and A.Z. Al-Garni

Friction welding of Al-Al, Al-steel, and steel-steel studs is compared. Transient heat generation and temperature rise during the welding process were modeled. Tensile tests and microhardness measurements across the weld zone were carried out. The metallurgical changes in the heat-affected zone were examined by SEM. Temperature rise at the interface plane was computed and related to weld properties. The affecting parameters on weld quality were identified by statistical analysis. Results show that interaction of weld parameters significantly affect yield, tensile, and breaking strength, and the heat-affected zone on the Al side is wider for Al-steel welds.

Keywords
friction welding, heat transfer

1. Introduction

FRICTION welding finds increasingly widespread industrial application as a mass production process for joining similar as well as dissimilar materials. The effect of process parameters on joint strength was studied by authors in Ref 1 and 2.

Friction welding refers to a group of nonfusion joining processes, in which a joint is produced by rotating one part against another while applying an axial force. Two types of friction welding use rotational motion. In the continuous-drive friction welding method, energy is supplied to the interface at constant rotational speed by an electric motor. In the inertia welding method, energy is derived from a flywheel of predetermined size, running at a predetermined initial speed.

In the continuous drive method, one of the components to be welded is held stationary while the other component is rotated at a specified speed. The two components are then brought together under axial pressure for a certain time period or until a predetermined burn-off is produced. The drive is then declutched, and the rotating component is quickly brought to a halt while the axial pressure is maintained or increased to a higher forging pressure.

In the inertia welding method, one of the components to be welded is held stationary while the second component is clamped in a spindle chuck, usually with attached flywheels. The flywheel and chuck assembly is then rotated to a certain speed to store a predetermined amount of energy. The drive to the flywheel is declutched, and the two components to be welded are brought together under axial pressure. Friction between the parts decelerates the flywheel converting stored energy to frictional heat.

Friction welding can be carried out at high production rates and, therefore, is economical in operation. In applications where friction welding has replaced other joining processes, the production rate has increased substantially (Ref 3). Savings in material also can be realized by friction welding; that is, less material is wasted in friction welding than in flash welding (Ref 4).

Cryogenic component welding for the JET project was carried out by Black (Ref 5), who reported the successful and economical process. Lewis (Ref 6) described some recent applications of friction welding and demonstrated the importance of control variables to weld quality. Nicholas (Ref 7) discussed the applicability of friction welding and showed some applications in compressors and valves.

A heat transfer mechanism taking place during friction welding was studied by Craine and Francis (Ref 8). They attempted to develop an analytical solution to the problem while assuming a continuous drive friction welding process. This assumption omits the transient nature of the process, because loading and forging processes are transiently carried out. Therefore their analysis fails to describe the real phenomena. This problem was later examined by Stokes (Ref 9) for the thermoplastic materials. He also assumed a steady state process and allowed the melting term in the heat transfer equation. However, this melting term may be needed for welding of thermoplastic materials, but it fails for metals because the interface temperature does not reach the melting temperature in the welding process. Consequently, a numerical scheme for the transient heating process taking place during friction welding becomes necessary.

The present study attempts to show a numerical solution for the transient heat transfer due to friction welding. Study is extended to include experimental investigation of welding parameters. Consequently, friction of similar and dissimilar materials is carried out. Experiment includes welding of Al, Al-steel, and steel bars. Different welding parameters are considered, including burn-off time, friction force, and forging load. The resulting welds are then subjected to mechanical tests; that is, microhardness and tensile tests. The metallurgical changes in the weld interface are examined by taking cross sections of weld zones. These cross sections are examined using scanning electron microscopy (SEM). Statistical analysis is introduced to identify the affecting parameters on weld strength in the friction welding process. These parameters include rotation speed, friction force, and burn-off time.

A.Z. Sahin, B.S. Yilbas, and **A.Z. Al-Garni,** Department of Mechanical Engineering, King Fahd University of Petroleum and Minerals, Dhahran 31261, Saudi Arabia.

2. Heat Transfer Analysis

Consider the two cylindrical bars with radius R are to be welded as shown in Fig. 1. The bars are assumed to be semi-infinite in z direction. Bar I is rotating with an angular velocity, ω, whereas bar II is stationary. At the surface of the intersection of the two bars, the coefficient of friction, μ, and the pressure, p, are assumed to be constant and uniform throughout the surface. The thermal diffusivities are α_1 for bar I and α_2 for bar II. Thermal conductivities and heat transfer coefficients are k_1 and h_1 for bar I and k_2 and h_2 for bar II. The transversal symmetry is also assumed to be satisfied.

This is a two-domain problem. Bar I is referred to as domain I, and bar II is referred to as domain II.

The formulation of the problem with the foregoing assumptions is:

$$\frac{\partial\theta}{\partial t}=\alpha_1\left[\frac{1}{r}\frac{\partial}{\partial r}\left(r\frac{\partial\theta}{\partial r}\right)+\frac{\partial^2\theta}{\partial z^2}\right] \quad \text{(Eq 1)}$$

$$\frac{\partial\phi}{\partial t}=\alpha_2\left[\frac{1}{r}\frac{\partial}{\partial r}\left(r\frac{\partial\phi}{\partial r}\right)+\frac{\partial^2\phi}{\partial z^2}\right] \quad \text{(Eq 2)}$$

$$\theta(r, z, 0)=0; \qquad \phi(r, z, 0)=0 \quad \text{(Eq 3)}$$

$$\frac{\partial\theta}{\partial z}(r, \infty, t)=0; \qquad \frac{\partial\phi}{\partial z}(r, -\infty, t)=0 \quad \text{(Eq 4)}$$

$$\frac{\partial\theta}{\partial r}(0, z, t)=0; \qquad \frac{\partial\phi}{\partial r}(0, z, t)=0 \quad \text{(Eq 5)}$$

$$\frac{\partial\theta}{\partial r}(R, z, t)-\frac{h_1}{k_1}\theta(R, z, t)=0$$

$$\frac{\partial\phi}{\partial r}(R, z, t)-\frac{h_2}{k_2}\phi(R, z, t)=0 \quad \text{(Eq 6)}$$

$$\theta(r, 0, t)=\phi(r, 0, t) \quad \text{(Eq 7)}$$

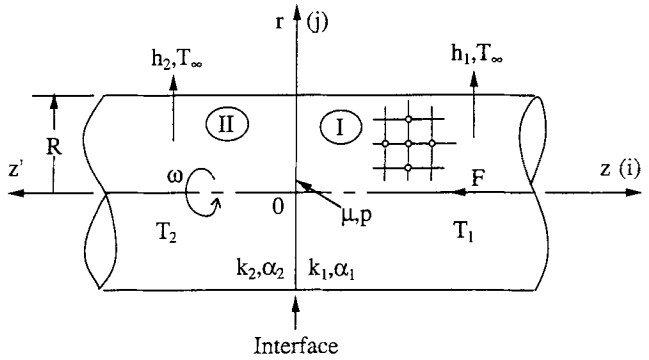

Fig. 1 Modeling of friction welding

$$-k_1\frac{\partial\theta}{\partial z}(r, 0, t)+\mu p(r)\omega r=-k_2\frac{\partial\phi}{\partial z}(r, 0, t) \quad \text{(Eq 8)}$$

where $\theta=T_1-T_\infty$ is the temperature in domain I, and $\phi=T_2-T_\infty$ is the temperature in domain II.

Using the nondimensional parameters; $\tau=\alpha_1 t/R^2$, $\rho=r/R$ and $\zeta=z/R$, $r_\alpha=\alpha_2/\alpha_1$, $r_k=k_2/k_1$, $B_1=h_1R/k_1$, and $B_2=h_2R/k_2$, the formulation of the problem in nondimensionalized form becomes:

$$\frac{\partial\theta}{\partial\tau}=\left[\frac{1}{\rho}\frac{\partial}{\partial\rho}\left(\rho\frac{\partial\theta}{\partial\rho}\right)+\frac{\partial^2\theta}{\partial\zeta^2}\right] \quad \text{(Eq 9)}$$

$$\frac{\partial\phi}{\partial\tau}=r_\alpha\left[\frac{1}{\rho}\frac{\partial}{\partial\rho}\left(\rho\frac{\partial\phi}{\partial\rho}\right)+\frac{\partial^2\phi}{\partial\zeta^2}\right] \quad \text{(Eq 10)}$$

$$\theta(\rho, \zeta, 0)=0; \qquad \phi(\rho, \zeta, 0)=0 \quad \text{(Eq 11)}$$

$$\frac{\partial\theta}{\partial\zeta}(\rho, \infty, \tau)=0; \qquad \frac{\partial\phi}{\partial\zeta}(\rho, -\infty, \tau)=0 \quad \text{(Eq 12)}$$

$$\frac{\partial\theta}{\partial\rho}(0, \zeta, \tau)=0; \qquad \frac{\partial\phi}{\partial\rho}(0, \zeta, \tau)=0 \quad \text{(Eq 13)}$$

$$\frac{\partial\theta}{\partial\rho}(1, \zeta, \tau)-B_1\theta(1, \zeta, \tau)=0;$$

$$\frac{\partial\phi}{\partial\rho}(1, \zeta, \tau)-B_2\phi(1, \zeta, \tau)=0 \quad \text{(Eq 14)}$$

$$\theta(\rho, 0, \tau)=\phi(\rho, 0, \tau) \quad \text{(Eq 15)}$$

$$-\frac{\partial\theta}{\partial\zeta}(\rho, 0, \tau)+\frac{\mu p\omega R^2}{k_1}=-r_k\frac{\partial\phi}{\partial\zeta}(\rho, 0, \tau) \quad \text{(Eq 16)}$$

3. Temperature Profile Solution

An analytical solution for the above problem is extremely difficult to obtain. Therefore, a finite difference technique is used to obtain the solution within a desired accuracy.

Assuming $\Delta z=\Delta r$ ($\Delta\zeta=\Delta\rho$), the following explicit form of finite difference formulation is obtained for a general node in domain I:

$$\theta'_{i,j}=\left[1-4\frac{\Delta\tau}{(\Delta\rho)^2}\right]\theta_{i,j}+\frac{\Delta\tau}{(\Delta\rho)^2}\left[\theta_{i-1,j}+\left(1-\frac{1}{2(j-1)}\right)\theta_{i,j-1}\right.$$

$$\left.+\left(1+\frac{1}{2j-1}\right)\theta_{i,j+1}+\theta_{i+1,j}\right] \quad \text{(Eq 17)}$$

for $i = 2, 3, \ldots, m$ and $j = 2, 3, \ldots, n$. $\theta_{i,j}'$ indicates the temperature of node (i, j) at time $\tau + \Delta\tau$.

In domain II, it is more convenient to use $z' = -z$ axis instead of z. Thus, the formulation becomes identical with domain I with the new set of thermophysical properties. If the same nondimensionalized parameters as employed in domain I are to be used, then the ratios of the thermophysical properties must be employed in the formulation, that is:

$$\phi_{i,j}' = \left[1 - 4\frac{r_\alpha \Delta\tau}{(\Delta\rho)^2}\right]\phi_{i,j} + \frac{r_\alpha \Delta\tau}{(\Delta\rho)^2}\left[\phi_{i-1,j} + \left(1 - \frac{1}{2(j-1)}\right)\phi_{i,j-1} + \left(1 + \frac{1}{2j-1}\right)\phi_{i,j+1} + \phi_{i+1,j}\right] \quad \text{(Eq 18)}$$

for $i = 2, 3, \ldots, m$ and $j = 2, 3, \ldots, n$.

Interface temperature variation is of particular interest in friction welding. Therefore, the finite difference equation that gives the interface temperature includes the diffusivities and conductivities of both domains and is given by means of ratios r_α and r_k.

$$\Theta_j' = \left[1 - 2(1 + r_k)\frac{2}{r_\alpha + r_k}\frac{r_\alpha \Delta\tau}{(\Delta\rho)^2}\right]\Theta_j + \frac{2}{r_\alpha + r_k}\frac{r_\alpha \Delta\tau}{(\Delta\rho)^2}\left[\theta_{1,j} + r_k\phi_{1,j} + \frac{1 + r_k}{2}\left(1 - \frac{1}{2(j-1)}\right)\Theta_{j-1} + \frac{1 + r_k}{2}\left(1 + \frac{1}{2(j-1)}\right)\Theta_{j+1} + \frac{\mu p \omega R^2}{k_1}(j-1)(\Delta\rho)^2\right] \quad \text{(Eq 19)}$$

for $j = 2, 3, \ldots, n$.

Stability of this explicit scheme is ensured by satisfying that:

$$1 - 4\frac{r_\alpha \Delta\tau}{(\Delta\rho)^2} \geq 0 \quad \text{(Eq 20)}$$

or

$$\frac{r_\alpha \Delta\tau}{(\Delta\rho)^2} \leq 0.25 \quad \text{(Eq 21)}$$

or

$$r_\alpha \Delta\tau \leq \frac{(\Delta\rho)^2}{4} \quad \text{(Eq 22)}$$

for any $r_\alpha > 1$. If $r_\alpha < 1$, then:

$$\Delta\tau \leq \frac{(\Delta\rho)^2}{4} \quad \text{(Eq 23)}$$

must be satisfied.

To facilitate the numerical solution of the thermal problem, heat transfer coefficients need to be determined. Being stationary, domain I experiences free convection with Grashoff number based on an average temperature of 600 K:

$$Gr = \frac{\beta g \Delta T D^3}{\nu^2}$$

estimated to be about 6000 within the experimental conditions. Under these conditions, the Nusselt number for domain I (Ref 10) is:

$$Nu_F = \frac{hD}{k} = 0.85(GrPr)^{0.188} = 4.056$$

and $\bar{h}_F = 19$ W/m$^2 \cdot$ K.

On the other hand, the Reynolds number for domain II, based on the peripheral velocity, is estimated to be 250. Since Re number is relatively small ($Gr \cong 0.5Re^2$), it is appropriate to consider both free and forced convection due to the rotation simultaneously. Nusselt number due to the rotation (Ref 11) is:

$$Nu_{rot} = 0.095Re^{2/3} = 3.74$$

and the combined effect of free and forced convection due to the rotation on the Nusselt number (Ref 10) is:

$$Nu_R = (Nu_F^3 + Nu_{rot}^3)^{1/3} = 4.92$$

which yields $\bar{h}_R = 23$ W/m$^2 \cdot$ K. Due to uncertainties, especially in the variation of surface temperature in the axial direction, this study considers $\bar{h}_F = 20$ W/m$^2 \cdot$ K for the stationary part (i.e., domain I) and $h_R = 25$ W/m$^2 \cdot$ K for the rotating part (i.e., domain II).

4. Experimental

Figure 2 shows experimental setup and force characteristics.

A computer controls the setup, which employs a hydraulic loading system. A computer controlled 10 kW alternating current (ac) driven electric motor with a maximum rotational speed of 3600 revolutions per minute (rpm) was used to rotate the workpiece. During the process, the friction period was determined by a burn-off length control device, which initiated the forge and arrest period when a preset amount of axial shortening had taken place. An infrared detector system was used to monitor the instantaneous temperature rise.

Two kinds of steel and one kind of Al were used as workpieces. The steel samples include H21 (DIN-X 30 W Cr V 93) and 1015 (DIN-1141), and Al samples include aluminum alloy 4032.

A wide range of machine settings was used in the initial trial of the experiment. These settings include burn-off time, rotational speed, breaking, and forge loads. The aim was to identify the combination of these settings, which gave welds that satis-

fied the mechanical tests. Table 1 gives these settings and their levels. A combination of the machine settings giving reproducible mechanical properties was selected for the remaining part of the study.

Before the melting process, Al sample surfaces were machined and degreased immediately prior to welding. The welding experiment was repeated three times at each combination of welding variables to provide sufficient specimens for testing and for checking the reproducibility of operation.

The mechanical tests, including tensile and microhardness tests, were carried out to assess the mechanical properties of the resulting welds. Cross sections of welds were subjected to microphotography using SEM to relate the mechanical properties with metallurgical characteristics.

Table 1 Welding parameters and their levels

Parameters	Level 1	Level 2	Level 3
Rotation speed, rpm	2000	2500	2800
Applied load, kg	500-1274	637-1783	764-2293
Welding duration, s	4	7	10

5. Statistical Testing

Factorial analysis is used to test the effects of the factors on the resulting weld properties. A complete factorial design is considered. Weld properties include tensile and yield strengths. The mathematical model governing the process is:

$$r_{i,j,k} = \mu + p_i + n_j + t_k + p_i \times n_j + n_j \times t_k + p_i \times t_k + \varepsilon_{i,j,k} \quad \text{(Eq 24)}$$

where $r_{i,j,k}$ represents the response (value given to the measured variable), μ is a common effect, p_i is the main effect of applied pressure, n_j is the main effect of the rotation speed, and t_k is the main effect of burn-off time. $p_i \times n_j$, $n_j \times t_k$, and $p_i \times t_k$ are the first-order interactions of applied pressure and rotation speed, rotation speed and burn-off time, and applied pressure and welding duration, respectively. $\varepsilon_{i,j,k}$ is the random error in the experiment, and i, j, k are the levels of applied pressure, rotation speed, and burn-off time, respectively. Table 1 gives the parameters and their levels. Further statistical arrangements of

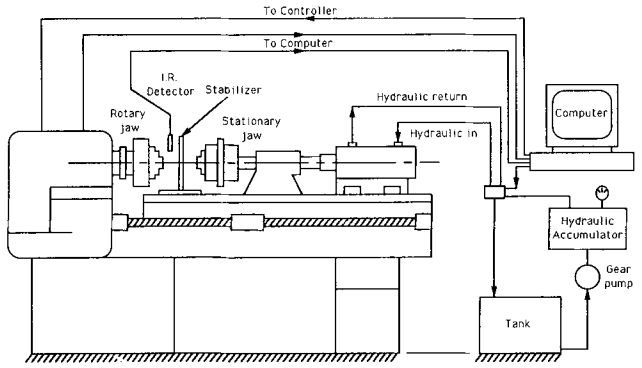

(a)

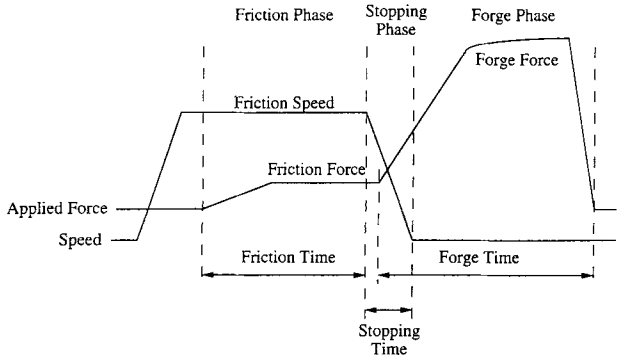

(b)

Fig. 2 (a) Experimental setup. (b) Forge-load characteristics

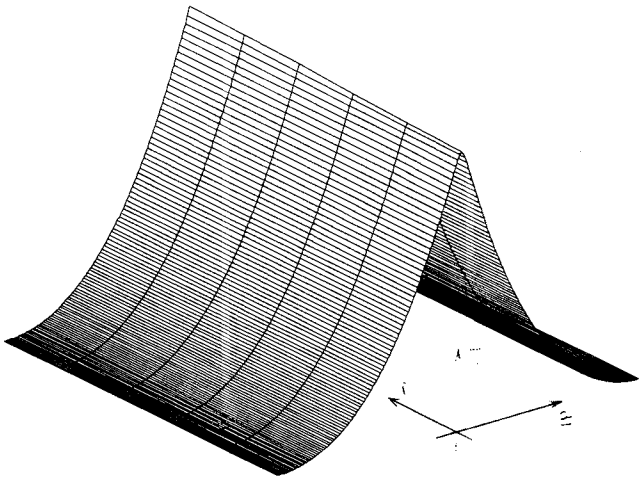

(a)

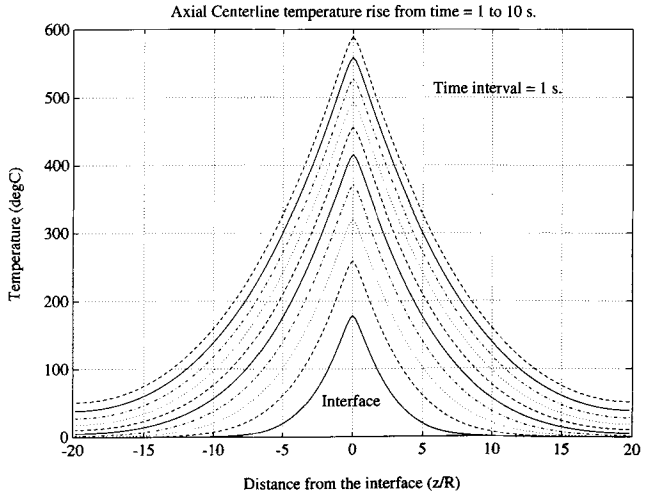

(b)

Fig. 3 (a) Three-dimensional mesh of temperature variation around the interface for Al-Al welds. (b) Temperature, distance, and time curves for Al-Al welds

this study are not given due to lengthy arguments involved (Ref 12).

Since the mathematical model for this analysis is a fixed and not a random model, the expected mean squares for the main effects are all estimates of the error mean variance. Therefore, the mean squares for the main effects can be compared with the error mean square to test the respective hypothesis by an F-test. The levels of significance in the present experiment are 5, 1, and 0.1% giving results that are significant, very significant, and most significant, respectively.

6. Discussion

Freshly machined components are used to avoid the contamination problem because oxide contamination reduces the weld quality; that is, in the rotational phase during welding, oxides can remain trapped and lack the close interface contact necessary to give full bonding.

During the experimentation and the heating model, rotation speed, applied friction load, and burn-off time determine the thermal conditions established at the weld zone while other parameters, such as burn-off length and forge load, influence the extent of interface consolidation. When rotational speed is reduced to its lowest value, weld quality drops, but it may be improved by increasing the burn-off length. The reverse trend exists at the highest welding speed where increased burn-off length gives rise to high weld zone temperature, which results in excessive material flow to sides from the welding zone. (See Fig. 15.)

Introducing additional breaking load to the rotating weld part during the arrest stage affects weld strength so that fast ar-

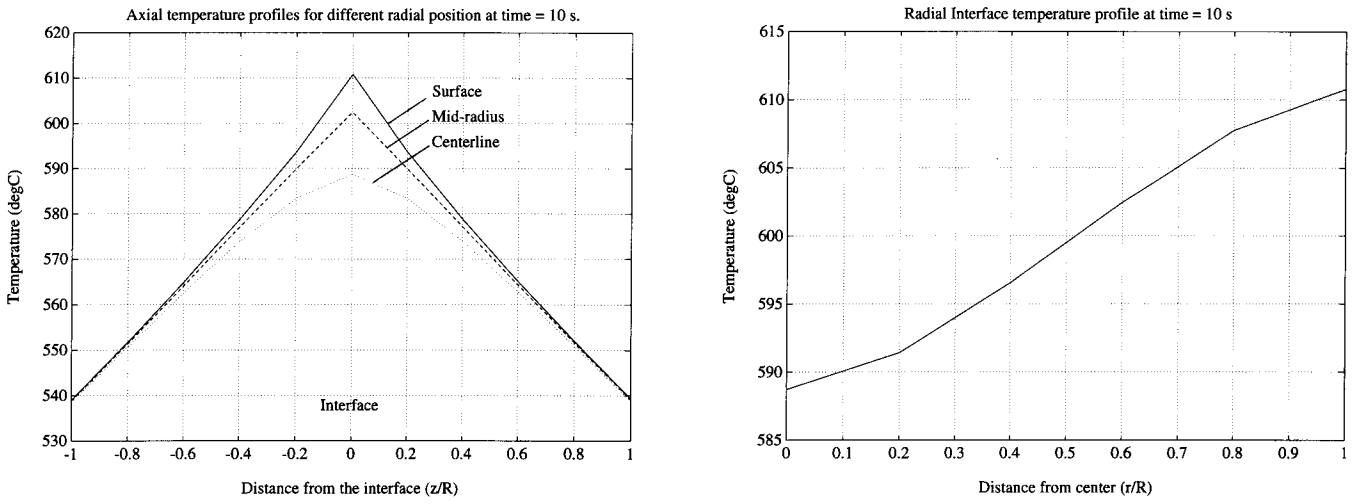

(a) (b)

Fig. 4 (a) Temperature variation along the axial distance from the interface for Al-Al welds. (b) Temperature variation along the interface for Al-Al welds

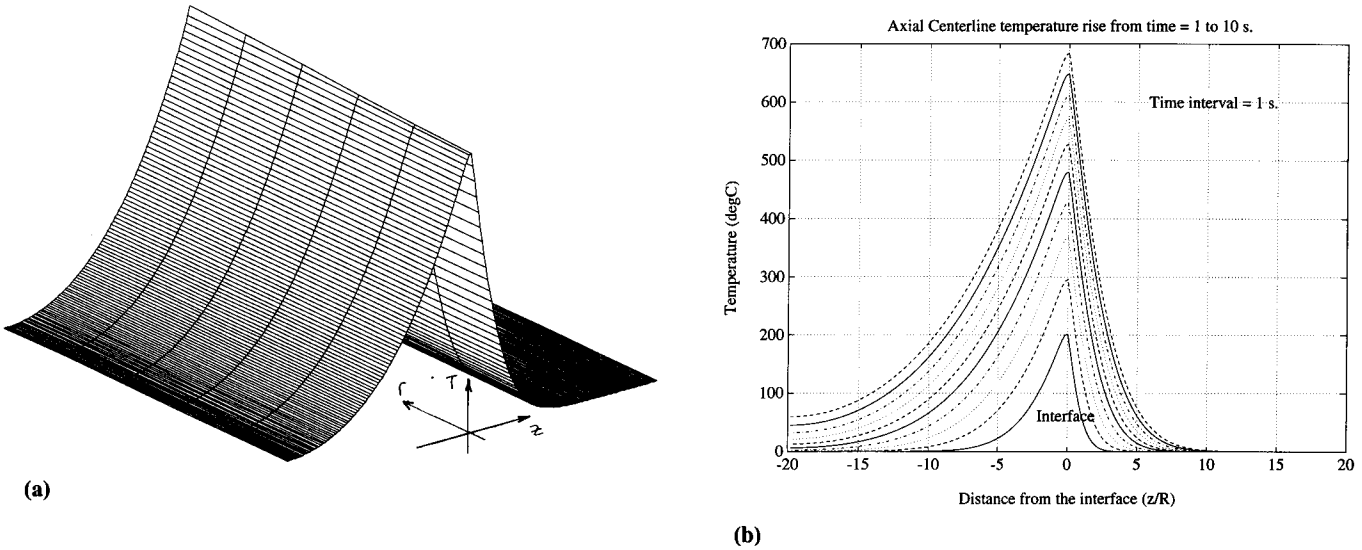

(a) (b)

Fig. 5 (a) Three-dimensional mesh of temperature variation around the interface for Al-Al welds. (b) Temperature, distance, and time curves for Al-H21 steel welds

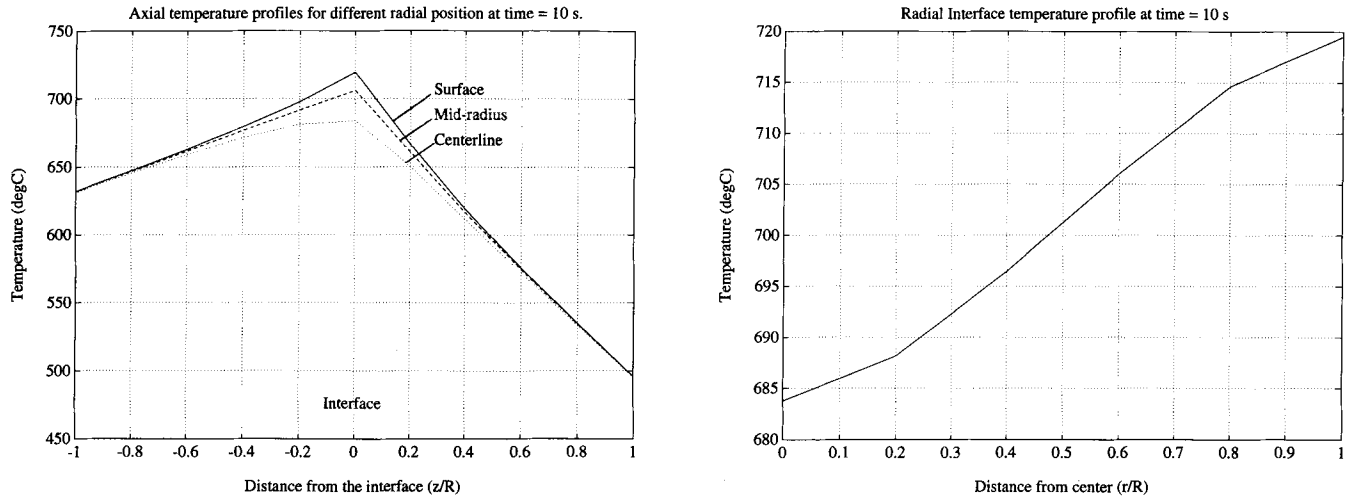

(a) (b)

Fig. 6 (a) Temperature variation along the axial distance from the interface for Al-H21 steel welds. (b) Temperature variation along the interface for Al-H21 steel welds

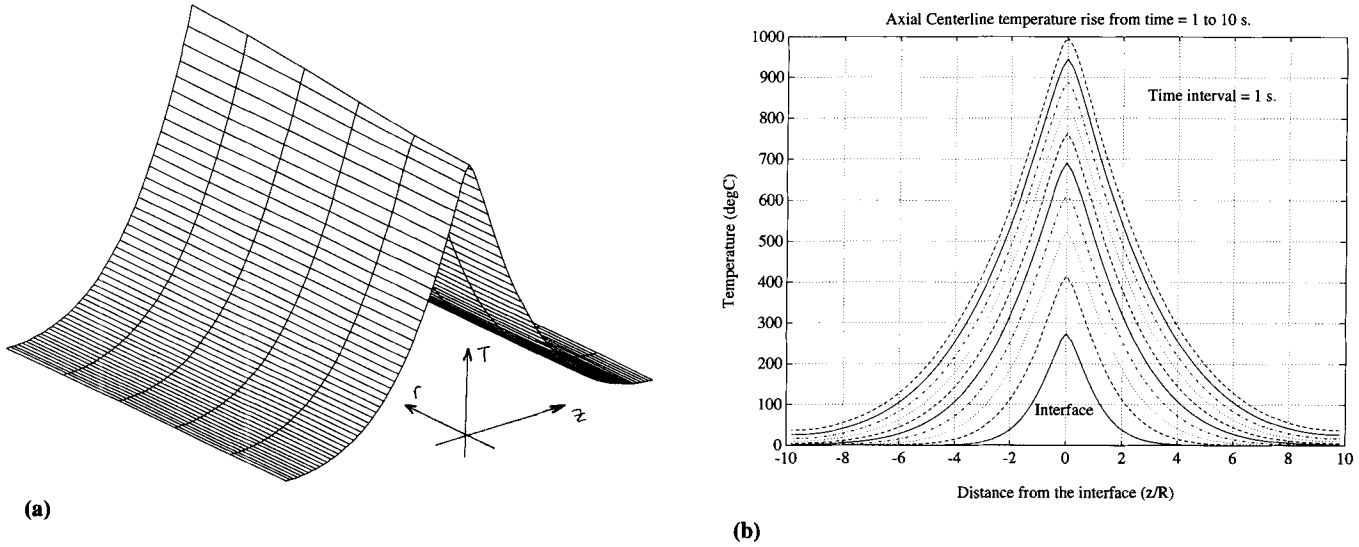

(a) (b)

Fig. 7 (a) Three-dimensional mesh of temperature variation around the interface for Al-Al welds. (b) Temperature, distance, and time curves for H21 steel-H21 steel welds

rest time lowers the weld tensile strength. Reduction in arrest time results in less forge displacement and reduces the arrest torque. Applying the arrest time long enough promotes both radial and tangential flow, which provide advantages for producing sound welds.

Table 2 shows the *F*-test result. The main effect of each parameter is less significant on the mechanical properties (yield, tensile, and breaking tensile strengths). Rotation speed, applied pressure, and burn-off time, individually, do not significantly affect the weld properties. On the other hand, the first-order interaction of these parameters significantly affects the resulting weld properties mentioned earlier. Hence, the coupling effects of these parameters are obvious on the weld properties. A simple, empirical formulation between the weld properties and these parameters, therefore, is rather difficult to obtain, which is also true for all the welds that employ similar or dissimilar material samples.

Frictional heat generated at the interface raises the workpiece temperature, over a very short axial distance, to a value approaching the melting range. If incipient melting occurs, there is little evidence in the resulting weld because the metal is worked during the welding stage. In the solution, both weld specimen surfaces are assumed to be free from any contamination, and friction coefficient is considered to be constant.

Figure 3 shows the variation of temperature, distance, and time curves in three-dimensional plot for Al-Al welds. Symmetrical temperature rise evidently occurs across the interface. Figure 3 provides a two-dimensional plot of this variation. Temperature rises rapidly at the interface, and as the distance

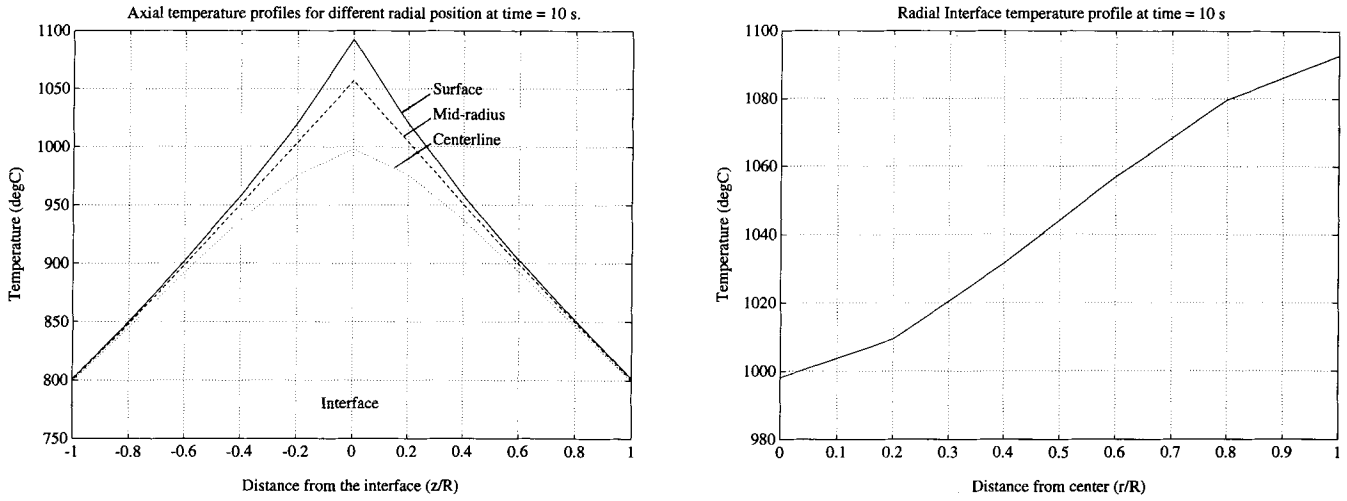

Fig. 8 (a) Temperature variation along the axial distance from the interface for H21 steel-H21 steel welds. (b) Temperature variation along the interface for H21 steel-H21 steel welds

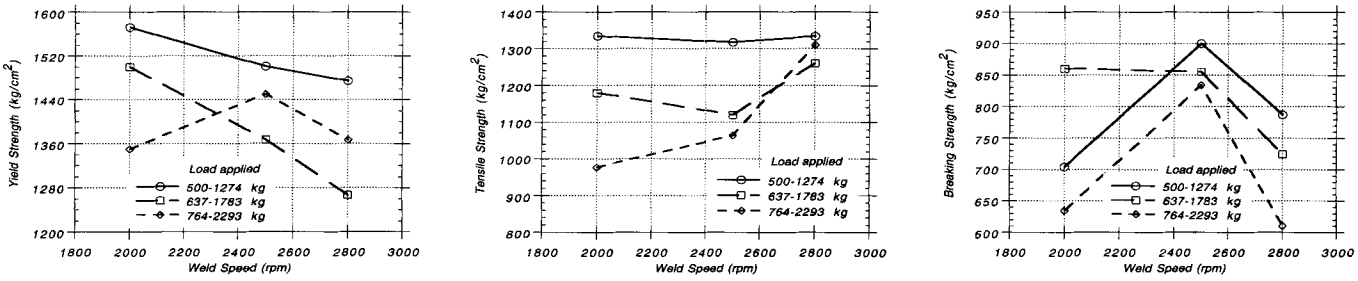

Fig. 9 Tensile test results for Al-Al welds

from the interface increases, temperature drops to room temperature. Heat generated at the interface due to friction, therefore, mainly increases the interface internal energy, and heat dissipated from the interface due to conduction and convection is small when compared to heat accumulated at the interface.

Figure 4 compares the results of temperature rise along the distance from interface. Temperature rises up to melting temperature at the mid-radius of the interface plane. However, temperature at the center of the interface plane is less than that at mid-radius and surface because heat generated by friction is relatively smaller than heat generated at the mid-radius and the surface. Heat generation is proportional to interface radius. On the other hand, temperature at the interface mid-radius is slightly less than temperature at the surface because of the convection effect. Rotational motion of the weld samples increases the convective heat transfer from the surface providing that this heat transfer slightly lowers the surface temperature (Fig. 4).

Figure 5 shows the three-dimensional plot of temperature, distance, and time curves for Al-steel welds. Nonsymmetrical temperature distribution occurs across the interface (Fig. 5). In this case, temperature drops rapidly in the steel side while it decays rather slowly in the Al side. This may be because Al has a relatively higher thermal diffusivity than steel. A larger heat-affected zone occurs on the Al side than on the steel side. In addition, interface temperature increases to around 700 °C, which in turn triggers the melting and/or softening of Al at the interface. This results in out flow of Al at the interface, which is also evident in Fig. 15. Temperature variation along the axial dis-

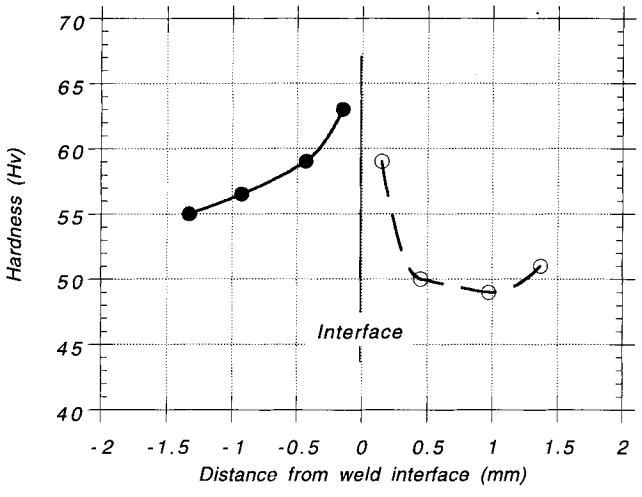

Fig. 10 Microhardness test results for Al-Al welds

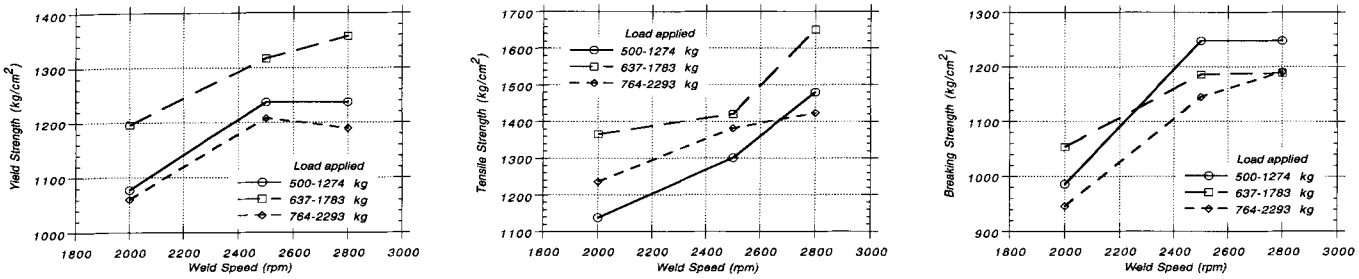

Fig. 11 Tensile test results for Al-H21 steel welds

Table 2 Statistical effects of weld parameters on mechanical properties

Parameters	Yield strength	Tensile strength	Breaking strength
Al-Al			
n	0.1 >	0.1 >	0.1 >
p	0.1 >	0.1 >	0.1 >
t	0.1 >	0.1 >	0.1 >
$n \times p$	0.01 <	0.01 <	0.01 <
$n \times t$	0.01 <	0.01 <	0.01 <
$p \times t$	0.01 <	0.01 <	0.01 <
Al-steel			
n	0.1 >	0.1 >	0.1 >
p	0.1 >	0.1 >	0.1 >
t	0.1 >	0.1 >	0.1 >
$n \times p$	0.01 <	0.01 <	0.1 >
$n \times t$	0.01 <	0.01 <	0.1 >
$p \times t$	0.01 <	0.01 <	0.1 >
Steel-steel			
n	0.1 >	0.1 >	0.1 >
p	0.1 >	0.1 >	0.1 >
t	0.1 >	0.1 >	0.1 >
$n \times p$	0.01 <	0.01 <	0.01 <
$n \times t$	0.01 <	0.01 <	0.01 <
$p \times t$	0.01 <	0.01 <	0.01 <

tance from the interface is shown in Fig. 6. Similar discussions apply as for Al-Al samples. Temperature at the interface gradually increases from center to surface. The slope of this increase from mid-radius to surface drops slightly due to the cooling effect of rotational motion during welding.

Figure 7 is a three-dimensional plot of temperature, distance, and time for steel-steel welding. Symmetrical temperatures across the interface occur. Maximum interface temperature rises to 1000 °C after 10 s of burn off. Therefore, melting at the interface is not attained. Temperature at the mid-radius is higher than at the center, but a little lower than at the surface, as shown in Fig. 8.

A comparison of Fig. 3, 5, and 7 shows a lower temperature rise in Al-Al welds than in both Al-steel and steel-steel welds. The heat-affected zone in the Al-steel welds is considerably wider on the Al side of the weld. This affects the mechanical properties of the resulting weld, such as tensile, yield, and breaking strength.

Figure 9 compares the yield, tensile, and breaking strength with weld speed for Al-Al welds. Tensile strength does not vary considerably with weld speed. It drops with increasing applied load because increased applied load results in out flow of Al

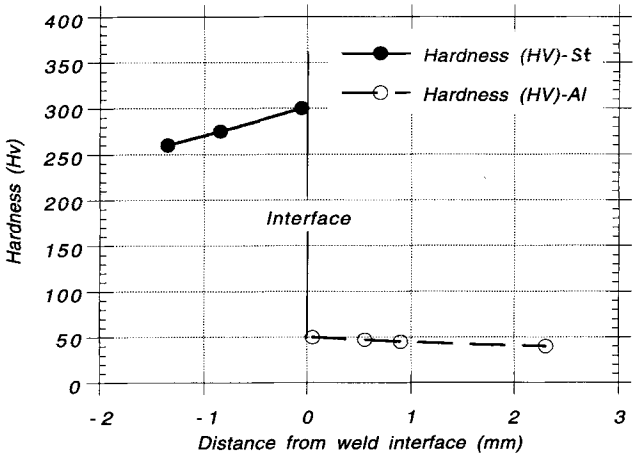

Fig. 12 Microhardness test results for Al-H21 steel welds

from the interface, which in turn develops rather weak bonds at the interface. This is also true with breaking strength. Yield strength decreases up to 15% with increasing weld speed. This may be explained in terms of the heat generation. The higher the rotational speed is, the higher the heat generation will be. Therefore, interface temperature increases, which results in softening of the metal at the interface. However, the cooling rate is high because of the high temperature attained. Therefore, yield strength drops.

Figure 10 shows microhardness test results for Al-Al welds. Hardness at the interface increases to 30 to 50%, and the heat-affected zone is about 1.5 mm across the interface. This may again be due to the amount of heat generation.

Figure 11 compares yield, tensile, and breaking strength with weld speed for Al-steel welds. Yield, tensile, and breaking strength of the resulting welds increase with increasing weld speed and decrease with increasing applied load. This may be due to the heat generation and cooling mechanism at the interface. Interface temperature increases substantially, and cooling rate is higher on the steel side than on the Al side. Consequently, in this case, increased heat generation improves weld strength.

Figure 12 shows the microhardness test results. Hardness increases at the interface because of heat generation. The heat-affected zone on the Al side is higher than on the steel side because of heat accumulation on the Al side during welding.

Figure 13 compares yield, tensile, and breaking strength with weld speed for steel-steel welds. Strength of the resulting

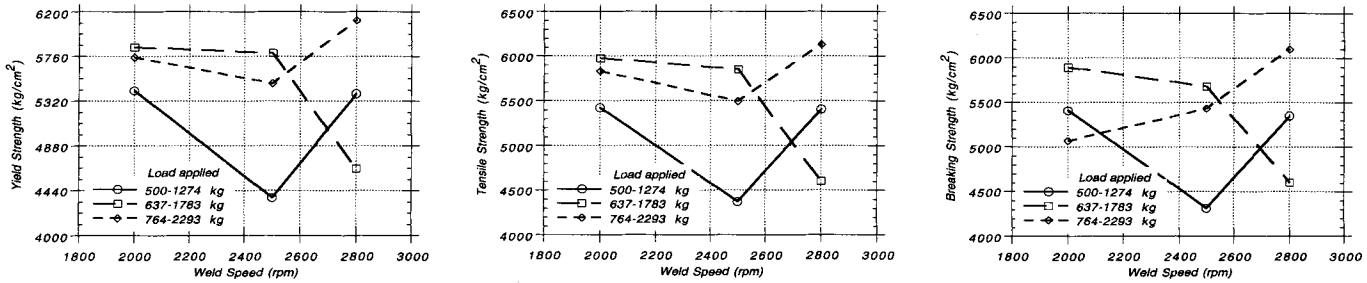

Fig. 13 Tensile test results for H21 steel-H21 steel welds

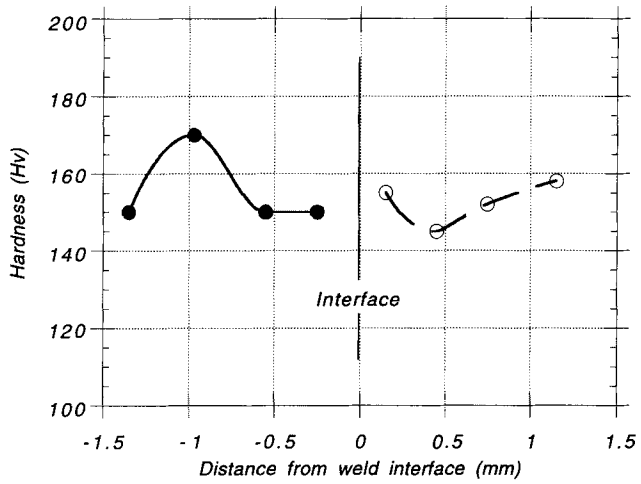

Fig. 14 Microhardness test results for friction welds joining 1015 steel and 1015 steel

welds varies with weld speed and applied load. Considerably higher strength is attained at all the weld speeds.

Microhardness test results are shown in Fig. 14 for steel-steel welds. Hardness drops at the interface and gradually increases at the outer edges of the heat-affected zone. Again the cause may be the heat generation and nature of the cooling mechanism.

A comparison of Fig. 9, 11, and 13 shows that weld strength of Al-steel is lower than that of Al-Al and steel-steel because of the heat transfer mechanism taking place between the interface and its surroundings. In this case, heat is accumulated in the Al side, and interface temperature is relatively higher than temperature for Al-Al welds. This argument is also supported from the microhardness test results. The heat-affected zone on the Al side is high for Al-steel welds.

Figure 15 shows the microphotographs of an Al-Al weld. Some degree of oxidation is evident because of high temperature. However, when the applied load is high, this oxide layer is broken into small compounds. Figure 16 is a microphotograph of an Al-steel weld. Intermetallic layer occurs at the interface. This extends only a 0.1 to 1 μm thickness from center to mid-radius, respectively. Surface contact of both samples causes no significant problem because Al is relatively soft. However, stable aluminum oxide develops a barrier to bond formation. Therefore, the times and temperatures required in diffusion are conducive to the formation and growth of intermetallics. Figure 17 is a microphotograph of a steel-steel weld. Bonding is almost perfect, and the heat-affected zone is only a fraction of a millimeter.

7. Conclusions

Factorial analysis results conclude that the main effects of all the welding parameters on yield, tensile, and breaking strengths are not significant. On the other hand, first-order interactions of these parameters significantly affect weld strength. Therefore, at some combination of friction force, rotational speed, and burn-off time, welding strength improves, but this varies with weld materials.

Temperature at the center of the interface plane is less than the temperature at mid-radius and surface. This is caused by heat generation, which is relatively small at the center. However, temperature at the mid-radius in the interface is slightly less than temperature at the surface because of the convection effect, which resulted from the rotational motion of the welds.

Temperature decay on the Al side is slower than that on the steel side for Al-steel welds. Heat accumulates on the Al side, which in turn increases the heat-affected zone on the Al side.

Tensile, yield, and breaking strengths of the welds are in the acceptable limits. Strength of Al-steel welds are relatively lower than those of Al-Al and steel-steel welds because of nonsymmetrical temperature distribution in the axial direction and attending high interface temperature.

Microhardness test results show that the heat-affected zone for all the welds is considerably narrow. For Al-steel welds, however, the heat-affected zone on the Al side is large. Microhardness increases at the interface for all the welds, except steel-steel welds. It drops; then it gradually increases because of the high temperature developed at the interface.

Microphotographs show that the aluminum oxide film is broken up into microcompounds, which in turn allow the exposure of the unaffected surface. In steel-steel welds, a bond, which developed at the interface, is very sound and gives rise to improved weld strength.

Acknowledgment

The authors acknowledge the support of King Fahd University of Petroleum and Minerals, Dhahran, Saudi Arabia for this work.

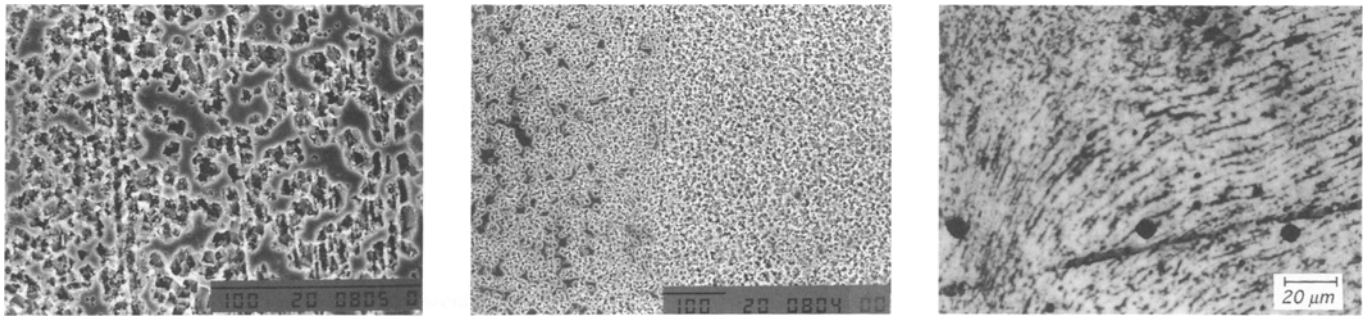

Fig. 15 Microphotographs of Al-Al weld

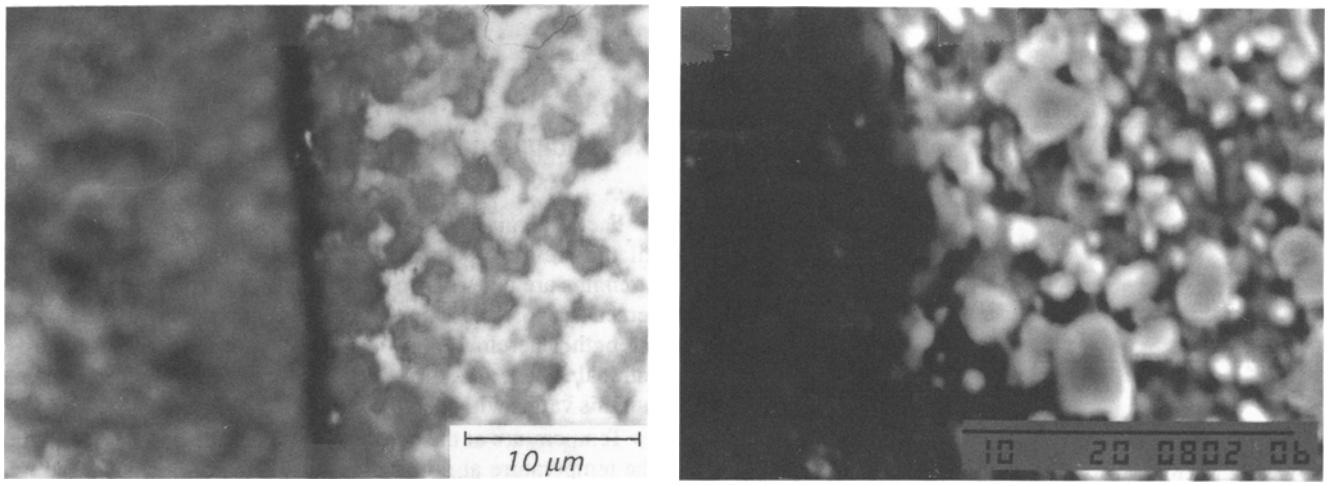

Fig. 16 Microphotographs of Al-1015 steel weld

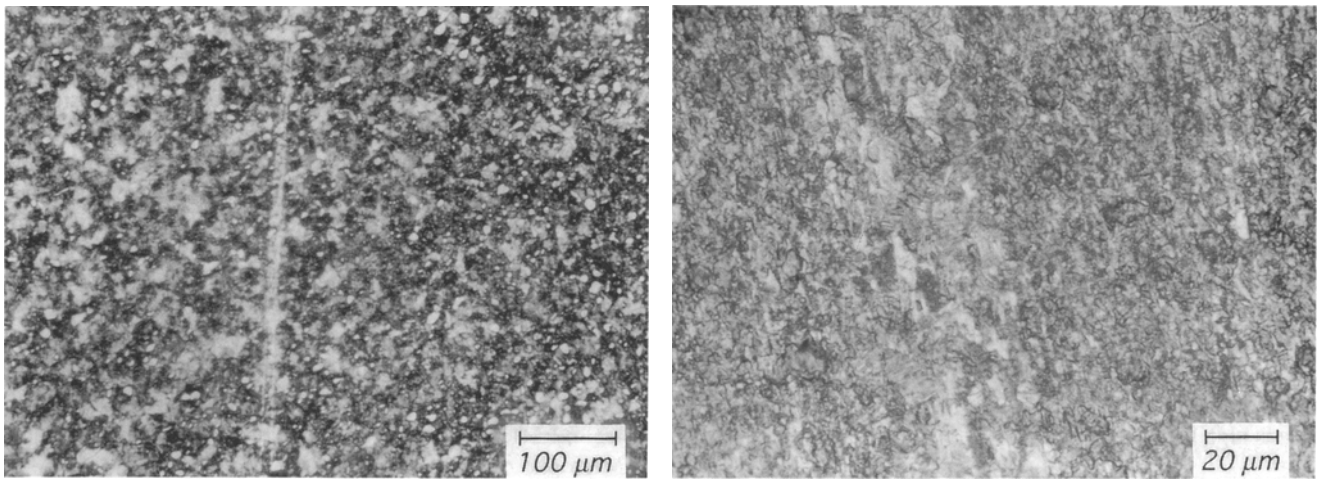

Fig. 17 Microphotographs of H21 steel-H21 steel weld

References

1. B.J. Eberhard, B.W. Schaaf, and A.D. Wilson, Friction Weld Ductility and Toughness as Influenced by Inclusion Morphology, *Weld. J.*, July 1983, p 171s-178s

2. B. Benn, Friction Welding of Butt Joints for High Duty Applications, *Weld. Met. Fabr.*, Aug/Sept 1988, p 284-286

3. J.M. Heberling, Building Strong Bonds with Inertia Welding, *Mach. Des.*, 6 Dec 1990, p 119-122

4. B.S. Yilbas, A.Z. Sahin, A. Coban, and B.J. Abdulaleem, Investigation into Properties of Friction Welding of Aluminum Bars, *J. Mater. Process. Technol., J. Special Volume-AMPT '93*, Vol 54 (No. 1-4), 1995, p 76-81

5. R.A. Black, Friction Welding Cryogenic Components for the JET Project, *Met. Constr.*, Sept 1983, p 574-576

Nomenclature

B	Biot number	T	Temperature, K
D	Diameter of rod, m	x	Measured variable
F	Variance ratio	z	Independent variable
g	Gravitational acceleration, m/s^2	α	Thermal diffusivity, m^2/s
Gr	Grasshoff number	β	Thermal expansion coefficient, 1/K
h	Heat transfer coefficient, $W/m^2 \cdot K$	μ	Coefficient of friction
k	Thermal conductivity, $W/m \cdot K$	ν	Dynamic viscosity, m^2/s
n	Rotation speed, 1/s	ω	Angular speed, 1/s
Nu	Nusselt number	ϕ	Temperature at domain II, K
p	Pressure, N/m^2	ρ	Dimensionless variable
Pr	Prandtl number	σ	Common effect
r	Independent variable	τ	Dimensionless time
R	Radius of rod, m	θ	Temperature at domain I, K
Re	Reynolds number	Θ	Temperature along the interface, K
r_α	Ratio of thermal diffusivities	ξ	Dimensionless variable
r_k	Ratio of thermal conductivities	ε	Random error
t	Time, s		

Subscripts

1	Domain I	F	Free
2.	Domain II	R	Rotation
∞	Ambient	s	Surface
c	Center	rot	Rotational

6. A. Lewis, Recent Developments in the Friction Welding Industry, *Weld. Met. Fabr.*, Aug/Sept 1989, p 289-293
7. E.D. Nicholas, Fabrication by Friction, *Fabr. Eng.*, April 1985, p 254-255
8. R.E. Craine and A. Francis, Frictional Heat Generated in the Early Stages of an Orbital Friction Welding Process, *Wear*, Vol 114, 1987, p 355-365
9. V.K. Stokes, Analysis of the Friction (Spin) Welding Process for Thermoplastics, *J. Mater. Sci.*, Vol 23, 1988, p 2772-2785
10. F.P. Incropera and D.P. Dewitt, *Introduction to Heat Transfer*, John Wiley & Sons, 1985
11. W.M. Kays and I.S. Bjorklund, Heat Transfer from a Rotating Cylinder with and without Crass-Flow, *Trans. ASME*, Vol 80 (No. 1), 1958, p 70-78
12. O.L. Dawies, *The Design and Analysis of Industrial Experiments*, Longman Group Ltd., 1978, p 245